Letter

Quantum skin Hall effect

Yuhao Ma and Taylor L. Hughes
Department of Physics, Institute for Condensed Matter Theory, and University of Illinois at Urbana-Champaign, Illinois 61801, USA

(Received 25 March 2022; accepted 21 June 2023; published 6 September 2023)

The skin effect, which is unique to non-Hermitian systems, can generate an extensive number of eigenstates localized near the boundary in an open geometry. Here, we propose that in two dimensions (2D) and three dimensions (3D) other quantities besides charge density are susceptible to the skin effect. We show that 2D and 3D models that are a hybrid between topological insulators and skin-effect systems can have a topological skin effect where an extensive number of topological modes, and the corresponding bulk topological invariant, are pinned to the surface. A key example, which we call the *quantum skin Hall effect* is constructed from layers of Chern insulators and exhibits an extensive Hall conductance and number of chiral modes bound to surfaces normal to the stack of layers. The same procedure is further extended to other symmetry classes to illustrate that a variety of one-dimensional and 2D topological invariants ($\mathbb{Z}$ or $\mathbb{Z}_2$) are subject to the skin effect. Indeed, we also propose a hybrid 2D system that exhibits an extensive number of topological corner modes and may be more easily realized in metamaterial experiments.

DOI: 10.1103/PhysRevB.108.L100301

The discovery of the skin effect [1–12] is a striking confirmation of the unusual character of non-Hermitian (NH) systems[13–15]. The conventional NH skin effect manifests in a macroscopic number of modes localized on the boundary of a system. In this article, we propose a three-dimensional (3D) *quantum skin Hall effect* where, instead of an extensive number of localized skin modes, we observe an extensive quantized Hall conductance pinned to the surface. Our effect can be generalized to show that a 3D system can exhibit a type of topological skin effect where an extensive amount of a variety of two-dimensional (2D) topological invariants, and their associated edge states, can be localized on the boundary. Since the NH skin effect has been successfully observed in mechanical [6,8,9], optical [10], and electronic systems [7,11], we expect our results may be experimentally realized imminently.

Recently there have been a number of investigations into the topological properties of NH systems, both theoretically [1–5,12,16–36] and experimentally [6–11,37–41]. Indeed, non-Hermiticity can be realized in various physical contexts: open systems [42,43], optics [44–47], quantum critical phenomena [48–50], and disordered or correlated systems [19,51,52]. Despite intense effort, integrating non-Hermiticity and topology has proved challenging, and many open questions remain. The key difficulty arises because of the dichotomy in the bulk-boundary correspondence. On one hand, the celebrated deterministic connection between bulk topological invariants and robust boundary modes is the cornerstone of topological insulator phenomena [53,54]. On the other hand, NH systems have an extreme sensitivity to boundary conditions such that most bulk properties in periodic boundary conditions (PBC) have no bearing on the phenomenology of systems with a boundary (OBC). The NH skin effect is the paradigm example of the boundary-condition sensitivity.

Here, we take a hybrid approach to combining non-Hermiticity and topology. We consider 2D/3D systems built from layers of one-dimensional (1D)/2D topological insulators that have non-Hermitian coupling between layers. In the Hermitian limit, these systems will exhibit a conventional bulk-boundary correspondence where the boundaries of the layers will exhibit topological modes that can hybridize and spread across the side surfaces [55]. Once non-Hermiticity is added, these topological boundary modes will experience a NH skin effect in the transverse direction that will pin all of the modes on the top and/or bottom surfaces. As we will see, when the 2D layer is a Chern insulator, this effect will generate an extensive number of chiral edge modes trapped at the top or bottom of a sample, and an associated extensive quantized Hall conductance. This construction can be generalized to other symmetry classes as well, e.g., time-reversal invariant (TRI) systems built from layers having a nontrivial $\mathbb{Z}_2$ invariant.

We begin by reviewing the translationally invariant 1D Hatano-Nelson (HN) model [56,57] [illustrated in Fig. 1(a)]. The HN model is a 1D single-band tight-binding model where non-Hermiticity is introduced via unequal hopping amplitudes in the left and right directions,

$$H_{HN} := \sum_i t_+ \hat{c}^\dagger_{i+1}\hat{c}_i + t_- \hat{c}^\dagger_i \hat{c}_{i+1}, \tag{1}$$

where $t_\pm = t \pm g$, $t > g$, and $g \in \mathbb{R}$. For PBC, the Bloch Hamiltonian is $H_{HN}(k) = t_+ e^{ik} + t_- e^{-ik}$, which, for any $g \neq 0$, has a complex spectrum in the shape of an ellipse that encloses the origin of the complex energy plane [shown in Fig. 1(b)].

A key development of the NH bulk-boundary correspondence is that the winding number $W(E)$ of the PBC spectrum around a complex energy E characterizes a so-called

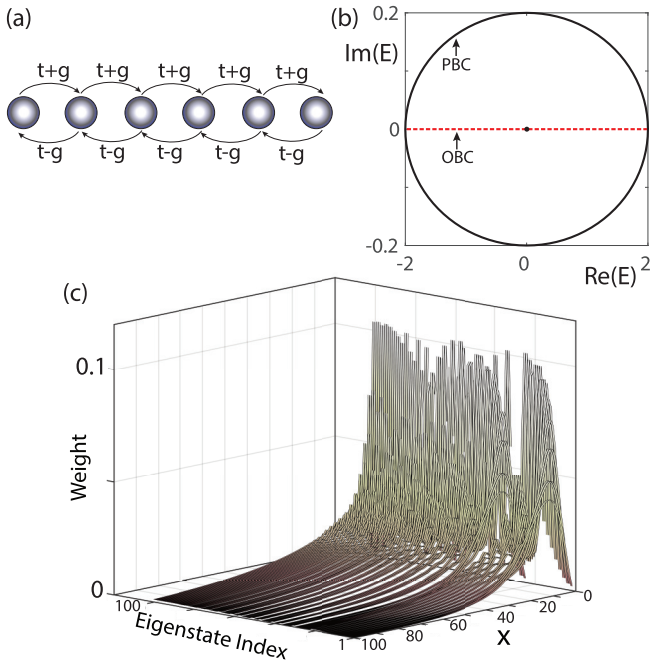

FIG. 1. (a) The Hatano-Nelson tight-binding model. (b) PBC bulk spectrum (black loop) and OBC spectrum (red dotted line) on the complex-energy plane, illustrating the high sensitivity of the system to its boundary conditions. (c) Spatial profile of all eigenstates vs lattice site index x in the OBC spectrum, showing the NH skin effect. Parameters: $t = 1, g = -0.1$.

"point-gap topology." If $W(E)$ is nonvanishing, it signals the existence of the NH skin effect in OBC [2,3]. The winding number is unique to NH systems as the spectrum of any Hermitian system lies completely on the real axis, making $W(E)$ ill defined. Specifically for the HN model, for any $E \in \mathbb{C}$ inside PBC spectral ellipse, the winding number is $W(E) = \mathrm{sgn}(g)$. We see that for $W(E)$ to change its value, g has to change its sign, during which the system will pass through the Hermitian limit such that the point gap closes. The sign of $W(E)$ indicates the side on which the skin modes are localized. Heuristically, if the sign of g is chosen to be negative, the hopping from right to left dominates and states flow to the left, and vice versa. As depicted in Fig. 1(c), for $g < 0$, every state in the OBC spectrum has its weight exponentially localized on the left half of the chain with a decay length controlled by the parameter t_-/t_+.

Having seen that the NH skin effect generates an extensive charge/mode density on the surface, it begs the question about what other physical quantities might be susceptible to a skin effect. Our approach to answering this question can be illustrated with a simple example. Suppose we have a stack of decoupled 2D topological insulator layers, all having a nontrivial topological invariant and associated edge states. If we couple them in the stacking direction then, in the order of increasing interlayer (Hermitian) coupling, we might arrive at a weak topological insulator [55,58], a topological semimetal [59,60], or a trivial insulator. However, if we modify the interlayer coupling using the HN model as a guide, we might expect that the extensive number of topological edge states, and the associated bulk topological phenomena, might be pushed to the top or bottom of the stack in a new type of NH skin effect.

To illustrate how we achieve this effect we will use a few examples, the first being a Chern insulator. We choose a simple two-band model for the 2D Chern insulator layer [61] having the Bloch Hamiltonian,

$$H_{\mathrm{Ch}}(\mathbf{k}) = \mathbf{h}(\mathbf{k}) \cdot \sigma, \tag{2}$$

where

$$\mathbf{h}(\mathbf{k}) = \left(\lambda \sin k_x,\ \lambda \sin k_y,\ m + \lambda \sum_{j=x,y} (1 - \cos k_j) \right), \tag{3}$$

and σ are the Pauli matrices for spin. We couple layers in the z direction using the NH terms,

$$H_{\mathrm{layer}} = \sum_{\alpha=\uparrow,\downarrow} \sum_{k_x,k_y,z} [(t+g)\hat{c}^\dagger_\alpha(k_x,k_y,z+1)\hat{c}_\alpha(k_x,k_y,z) + (t-g)\hat{c}^\dagger_\alpha(k_x,k_y,z)\hat{c}_\alpha(k_x,k_y,z+1)], \tag{4}$$

to end up with the full 3D Bloch Hamiltonian,

$$H_{\mathrm{3D}}(\mathbf{k}) = \epsilon(k_z)\mathbb{I}_{2\times 2} + \mathbf{h}(\mathbf{k}) \cdot \sigma, \tag{5}$$

where $\epsilon(k_z) = 2(t \cos k_z + ig \sin k_z) = t_+ e^{ik_z} + t_- e^{-ik_z}$.

Now, let us consider the properties of this model. The bulk energy bands in PBC are given by $E_\pm(\mathbf{k}) = \epsilon(k_z) \pm |\mathbf{h}(\mathbf{k})|$. In the Hermitian limit ($g = 0$) as we gradually turn on t when $\lambda = 1$, $2 < m < 4$, the bulk is gapped, and all the topological edge states initially localized on the edges of each decoupled layer will hybridize with each other and spread across the side surfaces. In Fig. 2(b) we zoom in to show the spectrum of the edge states (PBC in z, open in x, y) in the decoupled (blue stars) and weakly coupled cases (red dots), and show the clearly uniform distribution of the edge states on a yz surface plane in Fig. 2(c). As long as the amplitude of t is not large enough to close the bulk gap, the total number of edge state branches on each surface remains unchanged, i.e., remains equal to the number of z layers, and the system is a 3D weak topological Chern insulator. Although this is the regime on which we will focus, the intermediate coupling regime when t is stronger would result in a Weyl semimetal phase that would also be interesting to consider in future work.

Now, let us consider tuning away from the Hermitian limit. Because of the NH skin effect, we must be careful to study the properties of this system using various combinations of boundary conditions: (i) all directions periodic, (ii) z periodic, whereas, one or both of x, y open, (iii) z open, whereas, one or both of x, y open. Since the non-Hermiticity in the Bloch Hamiltonian is proportional to the identity matrix, the eigenstates for a periodic system in z are the same for all values of t, g. Hence, for case (i), we simply find a spectrum for the energy bands given in Eq. (5). For case (ii), we find that the edge state subbands that were broadened along the real energy axis by t will each form complex energy ellipses as shown in Figs. 2(a) and 2(b). Each ellipse has a nontrivial NH winding number around the region of real energies that were spanned in the $g = 0$ limit. Since z is periodic, the system retains its usual topological bulk-boundary correspondence yielding edge states distributed uniformly over the side surfaces, however, because of the spectral winding, we now know to

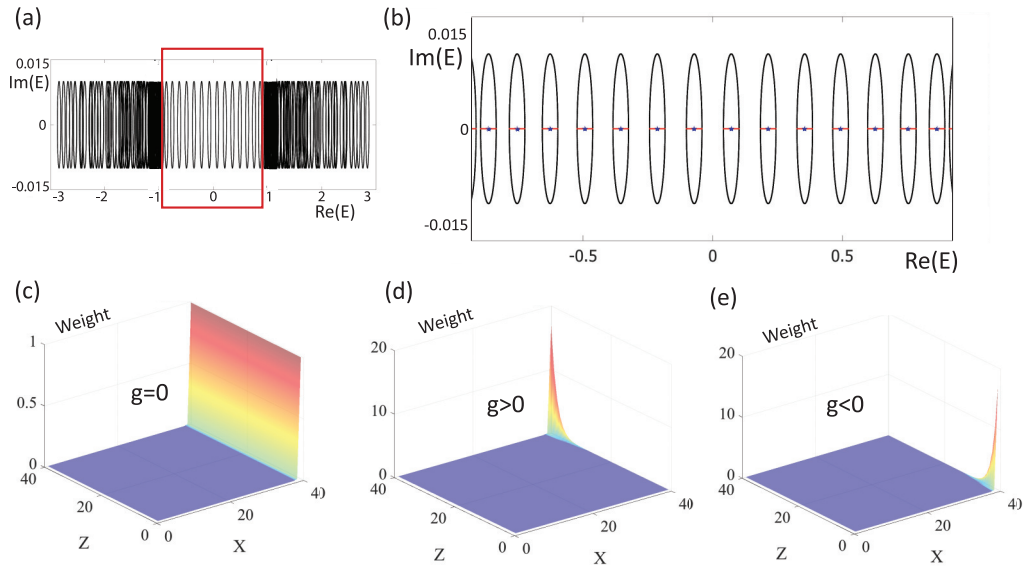

FIG. 2. (a) Complex energy spectrum with PBC in z, and OBC in x, y. (b) Zoom in on the boundary state region from (a) in red box. Blue stars have $t = g = 0$, red lines have $t \neq 0$, $g = 0$, and black lines have $t, g \neq 0$. (c)–(e) sum of probability densities of the negative Re(E) boundary states for (c)$g = 0$, (d) $g > 0$, and (e) $g < 0$.

expect a skin effect for all of the energy states in the spectrum. Indeed, for case (iii), where we expect to see strong effects of the non-Hermiticity, we find that the spectrum is real, and all the edge states are affected by a skin effect and, therefore, are exponentially localized on the top (bottom) surface for $g > 0$ ($g < 0$) as depicted in Figs. 2(d) and 2(e). This is in sharp contrast to the uniform distribution of the edge states in the Hermitian case shown in Fig. 2(c) (note the difference of scale in the weight among Figs. 2(d), 2(e), and 2(c).

In addition to characterizing the spectral features of our model, we will now identify a bulk manifestation of a quantum skin Hall effect via a Laughlin gauge argument [62]. To probe the quantum Hall effect, we will consider a system having open boundary conditions in x, z but periodic in y. Hence, we will thread a flux quantum in the periodic cycle in the y direction. Explicitly, we numerically evaluate the spatially resolved charge density as a function of flux $\Phi = \frac{h}{2\pi e}\theta$, $\theta \in [0, 2\pi]$, and then extract the amount of charge pumped in the x direction as a function of flux in the y direction (this is equivalent to applying an electric field in the y direction and measuring the Hall effect through a current in the x direction). For a system with $N_z = 20$ Chern insulator layers we find that the total charge transferred to the right side of the system when a single flux quantum is inserted is $|\Delta Q_R| = 20$ up to finite-size effects which introduce about a 2% error [see Fig. 3(a)]. The crucial feature of the quantum skin Hall effect is how this charge transfer is distributed among the layers as we show in Figs. 3(b) and 3(c). Indeed, Fig. 3(b) shows that the amount of charge transferred from one side of the system to the other is exponentially localized near the bottom or top surface depending on the sign of g. Additionally, Fig. 3(c) shows the total charge on each layer as a function of θ. In this figure, we can see an exponential localization of the total background charge in z, which represents the usual NH skin effect. Crucially, we also see that the flow of charge due to the quantum Hall effect, represented by the variation of the charge on top of the background, is also strongly layer dependent and dies out exponentially quickly as one moves away from the surface harboring the skin effect. The conclusion from the calculations in Figs. 2 and 3, is that that an extensive number of chiral edge states, and the associated quantized Hall conductance, are localized on the top or bottom surface.

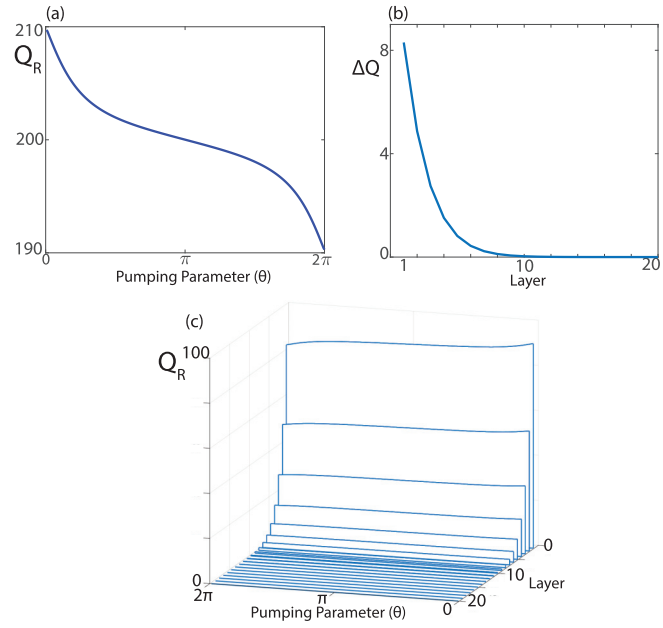

FIG. 3. (a) Total charge on the right half of the system (positive x direction) as a function of charge pumping parameter θ (i.e., the flux threaded in the y direction) for 20 Chern insulator layers. (b) An amount of charge pumped on each layer after one cycle. (c) Total charge on the right half of the system resolved vs layer. Note that the total charge is exponentially localized on one surface, and the variation of charge as a function of θ is strongest on that surface and decays away.

There have been multiple works regarding NH Chern insulators, which discover that the Hall conductance deviates from a quantized value [33–35] under different setups identified as Chern insulators by the NH topological band theory. This previous conclusion does not contradict with ours, here, since the non-Hermicity enters our model only through an identity matrix term. Thus, it does not effect the structure of the eigenstates and the conventional bulk-boundary correspondence is well preserved. Indeed, analyzing topology in NH systems generally requires both right and left eigenmodes, i.e., a biorthorgonal description [30,63]. However, such a formalism is unnecessary for our models since the non-Hermiticity enters only proportional to the identity matrix and, hence, can affect the spectrum, but does not affect the eigenmodes.

We expect our results to be generalizable to coupled layers of any type of topological system. For example, any topological insulator in 1D/2D that is layered into 2D/3D and has a Hatano-Nelson coupling between the layers should exhibit a hybrid bulk-boundary correspondence where topological modes are pushed to the transverse boundary via a NH skin effect. In the Chern insulator case, we have seen that chiral edge states pile up on the top or bottom, and since they are $\mathbb{Z}$ classified, we expect them to be stable as long as the bulk gap does not close. However, a possible complication may arise if the boundary states are $\mathbb{Z}_2$ classified, e.g., the helical edge modes on a quantum spin Hall (QSH) insulator or the 0D end states of a Su-Schrieffer-Heeger- (SSH-) type chain [64]. We will now argue that such systems have the same stability properties as their corresponding weak topological insulator counterparts, which are known to require a combination of internal symmetries and translation symmetry for protection [58].

To illustrate this, we can stack QSH insulators using a simple four-band model for the 2D TRI topological insulator layer [65] having the Bloch Hamiltonian,

$$H_{2\,\mathrm{DTI}}(\mathbf{k}) = A\sin(k_x)\Gamma^1 + A\sin(k_y)\Gamma^2 + M(\mathbf{k})\Gamma^0, \qquad (6)$$

where $M(\mathbf{k}) = M - B[2 - \cos(k_x) - \cos(k_x)]$, $\Gamma^1 = \sigma^x \otimes s^z$, $\Gamma^2 = -\sigma^y \otimes \mathbb{I}$, $\Gamma^0 = \sigma^z \otimes \mathbb{I}$, and σ^i/s^i are Pauli matrices acting on orbital/spin space. If we couple N_z layers using the Hatano-Nelson coupling [cf. Eq. (5)], we will generate an additional term $H = \epsilon(k_z)\mathbb{I}_{4\times4} + H_{2\,\mathrm{DTI}}(\mathbf{k})$. Hence, the spectrum for this model is effectively two copies of the stack of Chern insulators, we have already studied. For $g = 0$, the system is a TRI weak topological insulator with boundary states protected by time-reversal and translation symmetry. For finite g, the edge state spectra will form winding loops in complex energy space as in Figs. 2(a) and 2(b). In this scenario, an extensive number of helical modes will manifest on the top/bottom depending on the sign of g. If we break translation symmetry in the z direction, whereas, preserving time reversal, then we can dimerize the edge states and open a gap using a TRI coupling since they are $\mathbb{Z}_2$ classified. This will give rise to an even-odd effect where N_z being even/odd generically dictates zero/one stable helical edge state that will be pushed to the top or bottom by the NH skin effect. Hence, we find similar stability features to those of a 3D weak topological insulator. We note that we can also induce a bidirectional skin effect [see Fig. 4(a)] analogous to Ref. [3] where we use a modified NH interlayer coupling to arrive at

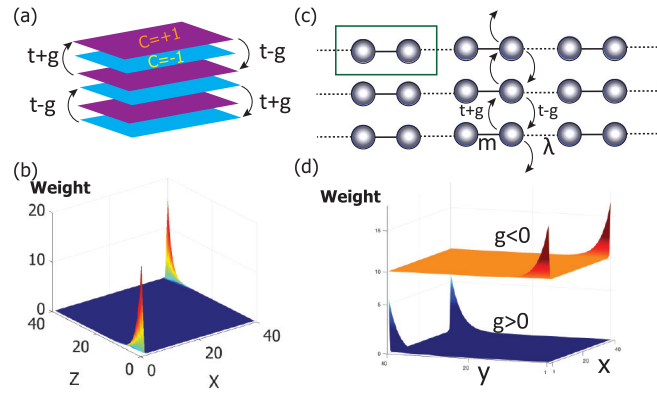

FIG. 4. (a) Schematic of a $\mathbb{Z}_2$ bidirectional skin effect model built from bilayers with opposite Chern number (b) the probability density of the negative energy boundary states at a fixed value of k_y for OBC in x, z and PBC in y. The subspace of boundary states at $-k_y$ would have the corners flipped. (c) Schematic of the 2D model built from Su-Schrieffer-Heeger chains parallel to $\hat{x}$ stacked with HN coupling along $\hat{y}$. (d) Probability density for negative energy boundary modes for OBC in x, y when $g < 0$ and $g > 0$. The plot for $g < 0$ has been manually shifted upward by a weight of 10 for easier visibility.

the Bloch Hamiltonian,

$$H_{bi}(\mathbf{k}) = 2t\,\cos(k_z)\mathbb{I}_{4\times4} + 2ig\,\sin(k_z)\mathbb{I}_{2\times2}\otimes s^z + H_{2\,\mathrm{DTI}}(\mathbf{k}). \qquad (7)$$

This model has a skin effect where an extensive number of edge states of one chirality appear on the top, whereas, the other chirality appears on the bottom, as shown in Fig. 4(b). The modified HN coupling breaks time-reversal and mirror in the z direction but preserves the product. We find that this effect survives even in the presence of symmetry-preserving terms that couple the opposite spin blocks, although the details of the spin content of the helical skin states will change.

As a final realization of this effect, let us consider a system more closely related to experiment. We will focus on a hybrid 2D system where we stack 1D inversion-symmetric SSH chains and then couple them with the HN coupling [see Fig. 4(c)]. Both the NH skin effect [6–11,37–41] and the SSH chain [66–69] have been realized in similar 1D metamaterial systems so their combination should be achievable in the near future. The Bloch Hamiltonian for this 2D model is

$$H(\mathbf{k}) = \epsilon(k_y)\mathbb{I}_{2\times2} + (m + \lambda\,\cos\,k_x)\sigma^x + \lambda\,\sin\,k_x\sigma^y. \qquad (8)$$

We can exhibit the interesting phenomenology of this model by tuning to the strongly dimerized limit $m = 0,\ \lambda = 1$. In periodic boundary conditions, this model has the spectrum $E_\pm(\mathbf{k}) = \epsilon(k_y) \pm 1$, which, for $t, g \neq 0$ is a pair of complex energy ellipses that are N_x-fold degenerate. With open boundaries along x, and with $t = g = 0$, there will be a pair of midgap modes on each SSH chain at zero energy, and completely localized on the end sites of the chains. Turning on t, g exactly realizes the usual 1D HN chain for the subspace of end states. Thus, we expect the boundary modes to exhibit a skin effect in the y direction such that for a fully open, square geometry there will be an extensive number of corner modes

on two of the four corners of the square [see Fig. 4(d)]. This is an unusual feature that would be a smoking-gun spectroscopoic signature for this hybrid topological skin effect phenomenon.

In addition to our newly proposed physical phenomena, we expect that the realization of our models may lead to useful engineering applications. The 1D NH skin effect has already been applied to create a funnel for light [70], and our 2D system of coupled SSH chains could be used as a combination of a signal splitter and a funnel where light impinging upon the system would be split and funneled along the two spatially separated edges. Additionally the extensive number of chiral modes associated to the 3D quantum skin Hall effect system could be used to enhance a topological laser [71,72], or as a kind of chiral funnel of light. The hybrid combination of topology transverse to the skin effect opens up a wide design space for new discoveries and applications.

We thank J. Claes and M. R. Hirsbrunner for useful discussions. We thank the U.S. Office of Naval Research (ONR) Multidisciplinary University Research Initiative (MURI) Grant No. N00014-20-1-2325 on Robust Photonic Materials with High-Order Topological Protection for support. We also thank the U.S. National Science Foundation (NSF) Emerging Frontiers in Research and Innovation (EFRI) Grant No. EFMA-1627184 for support.

[1] S. Yao and Z. Wang, Edge States and Topological Invariants of Non-Hermitian Systems, Phys. Rev. Lett. **121**, 086803 (2018).
[2] K. Zhang, Z. Yang, and C. Fang, Correspondence between Winding Numbers and Skin Modes in Non-Hermitian Systems, Phys. Rev. Lett. **125**, 126402 (2020).
[3] N. Okuma, K. Kawabata, K. Shiozaki, and M. Sato, Topological Origin of Non-Hermitian Skin Effects, Phys. Rev. Lett. **124**, 086801 (2020).
[4] C. H. Lee, L. Li, and J. Gong, Hybrid Higher-Order Skin-Topological Modes in Nonreciprocal Systems, Phys. Rev. Lett. **123**, 016805 (2019).
[5] C. H. Lee and R. Thomale, Anatomy of skin modes and topology in non-Hermitian systems, Phys. Rev. B **99**, 201103(R) (2019).
[6] A. Ghatak, M. Brandenbourger, J. van Wezel, and C. Coulais, Observation of non-Hermitian topology and its bulk-edge correspondence, Proc. Natl. Acad. Sci. USA **117**, 29561 (2020).
[7] T. Helbig, T. Hofmann, S. Imhof, M. Abdelghany, T. Kiessling, L. W. Molenkamp, C. H. Lee, A. Szameit, M. Greiter, and R. Thomale, Generalized bulkboundary correspondence in non-Hermitian topolectrical circuits, Nat. Phys. **16**, 747 (2020).
[8] M. Brandenbourger, X. Locsin, E. Lerner, and C. Coulais, Non-reciprocal robotic metamaterials, Nat. Commun. **10**, 4608 (2019).
[9] D. Zhou and J. Zhang, Non-Hermitian topological metamaterials with odd elasticity, Phys. Rev. Res. **2**, 023173 (2020).
[10] L. Xiao, T. Deng, K. Wang, G. Zhu, Z. Wang, W. Yi, and P. Xue, Non-Hermitian bulk–boundary correspondence in quantum dynamics, Nat. Phys. **16**, 761 (2020).
[11] T. Hofmann, T. Helbig, F. Schindler, N. Salgo, M. Brzezińska, M. Greiter, T. Kiessling, D. Wolf, A. Vollhardt, A. Kabaši *et al.*, Reciprocal skin effect and its realization in a topolectrical circuit, Phys. Rev. Res. **2**, 023265 (2020).
[12] F. Song, S. Yao, and Z. Wang, Non-Hermitian Skin Effect and Chiral Damping in Open Quantum Systems, Phys. Rev. Lett. **123**, 170401 (2019).
[13] C. M. Bender and S. Boettcher, Real Spectra in Non-Hermitian Hamiltonians Having $\mathcal{PT}$ Symmetry, Phys. Rev. Lett. **80**, 5243 (1998).
[14] C. M. Bender, S. Boettcher, and P. N. Meisinger, $\mathcal{PT}$-symmetric quantum mechanics, J. Math. Phys. **40**, 2201 (1999).
[15] C. M. Bender, Making sense of non-Hermitian Hamiltonians, Rep. Prog. Phys. **70**, 947 (2007).
[16] Y. C. Hu and T. L. Hughes, Absence of topological insulator phases in non-Hermitian $\mathcal{PT}$-symmetric Hamiltonians, Phys. Rev. B **84**, 153101 (2011).
[17] Z. Gong, Y. Ashida, K. Kawabata, K. Takasan, S. Higashikawa, and M. Ueda, Topological Phases of Non-Hermitian Systems, Phys. Rev. X **8**, 031079 (2018).
[18] K. Kawabata, S. Higashikawa, Z. Gong, Y. Ashida, and M. Ueda, Topological unification of time-reversal and particle-hole symmetries in non-Hermitian physics, Nat. Commun. **10**, 297 (2019).
[19] R. Hamazaki, K. Kawabata, and M. Ueda, Non-Hermitian Many-Body Localization, Phys. Rev. Lett. **123**, 090603 (2019).
[20] B. Zhu, R. Lü, and S. Chen, $\mathcal{PT}$ symmetry in the non-Hermitian Su-Schrieffer-heeger model with complex boundary potentials, Phys. Rev. A **89**, 062102 (2014).
[21] C. Yin, H. Jiang, L. Li, R. Lü, and S. Chen, Geometrical meaning of winding number and its characterization of topological phases in one-dimensional chiral non-Hermitian systems, Phys. Rev. A **97**, 052115 (2018).
[22] S. Lieu, Topological phases in the non-Hermitian Su-Schrieffer-Heeger model, Phys. Rev. B **97**, 045106 (2018).
[23] K. Kawabata, T. Bessho, and M. Sato, Classification of Exceptional Points and Non-Hermitian Topological Semimetals, Phys. Rev. Lett. **123**, 066405 (2019).
[24] K. Kawabata, K. Shiozaki, M. Ueda, and M. Sato, Symmetry and Topology in Non-Hermitian Physics, Phys. Rev. X **9**, 041015 (2019).
[25] H. Zhou and J. Y. Lee, Periodic table for topological bands with non-Hermitian symmetries, Phys. Rev. B **99**, 235112 (2019).
[26] J. C. Budich, J. Carlström, F. K. Kunst, and E. J. Bergholtz, Symmetry-protected nodal phases in non-Hermitian systems, Phys. Rev. B **99**, 041406(R) (2019).
[27] T.-S. Deng and W. Yi, Non-bloch topological invariants in a non-Hermitian domain wall system, Phys. Rev. B **100**, 035102 (2019).
[28] K. Yokomizo and S. Murakami, Non-Bloch Band Theory of Non-Hermitian Systems, Phys. Rev. Lett. **123**, 066404 (2019).
[29] T. E. Lee, Anomalous Edge State in a Non-Hermitian Lattice, Phys. Rev. Lett. **116**, 133903 (2016).

[30] H. Shen, B. Zhen, and L. Fu, Topological Band Theory for Non-Hermitian Hamiltonians, Phys. Rev. Lett. **120**, 146402 (2018).

[31] K. Kawabata, Y. Ashida, H. Katsura, and M. Ueda, Parity-time-symmetric topological superconductor, Phys. Rev. B **98**, 085116 (2018).

[32] S. Yao, F. Song, and Z. Wang, Non-Hermitian Chern Bands, Phys. Rev. Lett. **121**, 136802 (2018).

[33] Y. Chen and H. Zhai, Hall conductance of a non-Hermitian chern insulator, Phys. Rev. B **98**, 245130 (2018).

[34] T. M. Philip, M. R. Hirsbrunner, and M. J. Gilbert, Loss of hall conductivity quantization in a non-Hermitian quantum anomalous Hall insulator, Phys. Rev. B **98**, 155430 (2018).

[35] M. R. Hirsbrunner, T. M. Philip, and M. J. Gilbert, Topology and observables of the non-Hermitian Chern insulator, Phys. Rev. B **100**, 081104(R) (2019).

[36] S. Groenendijk, T. L. Schmidt, and T. Meng, Universal hall conductance scaling in non-Hermitian Chern insulators, Phys. Rev. Res. **3**, 023001 (2021).

[37] L. Xiao, X. Zhan, Z. Bian, K. Wang, X. Zhang, X. Wang, J. Li, K. Mochizuki, D. Kim, N. Kawakami *et al.*, Observation of topological edge states in parity–time-symmetric quantum walks, Nat. Phys. **13**, 1117 (2017).

[38] S. Weimann, M. Kremer, Y. Plotnik, Y. Lumer, S. Nolte, K. G. Makris, M. Segev, M. C. Rechtsman, and A. Szameit, Topologically protected bound states in photonic parity–time-symmetric crystals, Nature Mater. **16**, 433 (2017).

[39] H. Zhao, P. Miao, M. H. Teimourpour, S. Malzard, R. El-Ganainy, H. Schomerus, and L. Feng, Topological hybrid silicon microlasers, Nat. Commun. **9**, 1 (2018).

[40] M. Parto, S. Wittek, H. Hodaei, G. Harari, M. A. Bandres, J. Ren, M. C. Rechtsman, M. Segev, D. N. Christodoulides, and M. Khajavikhan, Complex edge-state phase transitions in 1D topological laser arrays, in *CLEO: QELS_Fundamental Science* (Optica Publishing Group, Optical Society of America, 2018), pp. FM2E–5.

[41] X. Zhan, L. Xiao, Z. Bian, K. Wang, X. Qiu, B. C. Sanders, W. Yi, and P. Xue, Detecting Topological Invariants in Nonunitary Discrete-Time Quantum Walks, Phys. Rev. Lett. **119**, 130501 (2017).

[42] V. V. Konotop, J. Yang, and D. A. Zezyulin, Nonlinear waves in $\mathcal{PT}$-symmetric systems, Rev. Mod. Phys. **88**, 035002 (2016).

[43] R. El-Ganainy, K. G. Makris, M. Khajavikhan, Z. H. Musslimani, S. Rotter, and D. N. Christodoulides, Non-Hermitian physics and $\mathcal{PT}$ symmetry, Nat. Phys. **14**, 11 (2018).

[44] L. Feng, R. El-Ganainy, and L. Ge, Non-Hermitian photonics based on parity–time symmetry, Nat. Photon. **11**, 752 (2017).

[45] M.-A. Miri and A. Alu, Exceptional points in optics and photonics, Science **363**, eaar7709(2019).

[46] S. Malzard, C. Poli, and H. Schomerus, Topologically Protected Defect States in Open Photonic Systems with Non-Hermitian Charge-Conjugation and Parity-Time Symmetry, Phys. Rev. Lett. **115**, 200402 (2015).

[47] K. Mochizuki, D. Kim, and H. Obuse, Explicit definition of $\mathcal{PT}$ symmetry for nonunitary quantum walks with gain and loss, Phys. Rev. A **93**, 062116 (2016).

[48] K. Kawabata, Y. Ashida, and M. Ueda, Information Retrieval and Criticality in Parity-Time-Symmetric Systems, Phys. Rev. Lett. **119**, 190401 (2017).

[49] M. Nakagawa, N. Kawakami, and M. Ueda, Non-Hermitian Kondo Effect in Ultracold Alkaline-Earth Atoms, Phys. Rev. Lett. **121**, 203001 (2018).

[50] L. Xiao, K. Wang, X. Zhan, Z. Bian, K. Kawabata, M. Ueda, W. Yi, and P. Xue, Observation of Critical Phenomena in Parity-Time-Symmetric Quantum Dynamics, Phys. Rev. Lett. **123**, 230401 (2019).

[51] T. Yoshida, R. Peters, N. Kawakami, and Y. Hatsugai, Symmetry-protected exceptional rings in two-dimensional correlated systems with chiral symmetry, Phys. Rev. B **99**, 121101(R) (2019).

[52] A. A. Zyuzin and A. Y. Zyuzin, Flat band in disorder-driven non-Hermitian Weyl semimetals, Phys. Rev. B **97**, 041203(R) (2018).

[53] M. Z. Hasan and C. L. Kane, Colloquium: Topological insulators, Rev. Mod. Phys. **82**, 3045 (2010).

[54] B. A. Bernevig and T. L. Hughes, *Topological Insulators and Topological Superconductors* (Princeton University Press, Princeton, NJ. 2013).

[55] L. Balents and M. P. A. Fisher, Chiral Surface States in the Bulk Quantum Hall Effect, Phys. Rev. Lett. **76**, 2782 (1996).

[56] N. Hatano and D. R. Nelson, Localization Transitions in Non-Hermitian Quantum Mechanics, Phys. Rev. Lett. **77**, 570 (1996).

[57] N. Hatano and D. R. Nelson, Vortex pinning and non-Hermitian quantum mechanics, Phys. Rev. B **56**, 8651 (1997).

[58] L. Fu, C. L. Kane, and E. J. Mele, Topological Insulators in Three Dimensions, Phys. Rev. Lett. **98**, 106803 (2007).

[59] A. A. Burkov, M. D. Hook, and L. Balents, Topological nodal semimetals, Phys. Rev. B **84**, 235126 (2011).

[60] S. T. Ramamurthy and T. L. Hughes, Patterns of electromagnetic response in topological semimetals, Phys. Rev. B **92**, 085105 (2015).

[61] X.-L. Qi, Y.-S. Wu, and S.-C. Zhang, Topological quantization of the spin Hall effect in two-dimensional paramagnetic semiconductors, Phys. Rev. B **74**, 085308 (2006).

[62] R. B. Laughlin, Quantized Hall conductivity in two dimensions, Phys. Rev. B **23**, 5632 (1981).

[63] F. K. Kunst, E. Edvardsson, J. C. Budich, and E. J. Bergholtz, Biorthogonal Bulk-Boundary Correspondence in Non-Hermitian Systems, Phys. Rev. Lett. **121**, 026808 (2018).

[64] W.-P. Su, J. R. Schrieffer, and A. J. Heeger, Soliton excitations in polyacetylene, Phys. Rev. B **22**, 2099 (1980).

[65] B. A. Bernevig, T. L. Hughes, and S.-C. Zhang, Quantum spin hall effect and topological phase transition in HgTe quantum wells, Science **314**, 1757 (2006).

[66] N. Malkova, I. Hromada, X. Wang, G. Bryant, and Z. Chen, Observation of optical shockley-like surface states in photonic superlattices, Opt. Lett. **34**, 1633 (2009).

[67] T. Eichelkraut, R. Heilmann, S. Weimann, S. Stützer, F. Dreisow, D. N. Christodoulides, S. Nolte, and A. Szameit, Mobility transition from ballistic to diffusive transport in non-Hermitian lattices, Nat. Commun. **4**, 2533 (2013).

[68] J. M. Zeuner, M. C. Rechtsman, Y. Plotnik, Y. Lumer, S. Nolte, M. S. Rudner, M. Segev, and A. Szameit, Observation of a Topological Transition in the Bulk of a Non-Hermitian System, Phys. Rev. Lett. **115**, 040402 (2015).

[69] C.-H. Lee, S. Imhof, C. Berger, F. Bayer, J. Brehm, L. W. Molenkamp, T. Kiessling, and R. Thomale, Topolectrical circuits, Commun. Phys. **1**, 39 (2018).

[70] S. Weidemann, M. Kremer, T. Helbig, T. Hofmann, A. Stegmaier, M. Greiter, R. Thomale, and A. Szameit, Topological funneling of light, Science **368**, 311 (2020).

[71] G. Harari, M. A. Bandres, Y. Lumer, M. C. Rechtsman, Y. D. Chong, M. Khajavikhan, D. N. Christodoulides, and M. Segev, Topological insulator laser: Theory, Science **359**, eaar4003(2018).

[72] M. A. Bandres, S. Wittek, G. Harari, M. Parto, J. Ren, M. Segev, D. N. Christodoulides, and M. Khajavikhan, Topological insulator laser: Experiments, Science **359**, eaar4005(2018).